Journal of Fluids and Structures (2001) **15,** 327–350
doi:10.1006/jfls.2000.0343, available online at http://www.idealibrary.com on IDEAL®

NUMERICAL SIMULATION OF FLOW INTERFERENCE BETWEEN TWO CIRCULAR CYLINDERS IN TANDEM AND SIDE-BY-SIDE ARRANGEMENTS

J. R. Meneghini, F. Saltara

Department of Mechanical Engineering, University of São Paulo, Brazil

C. L. R. Siqueira

Department of Naval Engineering, University of São Paulo, Brazil

AND

J. A. Ferrari Jr

Petrobrás, Rio de Janeiro, Brazil

(Received 23 September 1999, and in final form 26 October 2000)

The shedding of vortices and flow interference between two circular cylinders in tandem and side-by-side arrangements are investigated numerically in this paper. A *Fractional Step Method* is used for the simulations and the flow is assumed two-dimensional. The calculations are carried out on a three-noded unstructured mesh. The simulations are performed for a Reynolds number range varying from 100 to 200, and the flow is solved through the finite-element method. The mesh is finer close to the cylinder wall in order to have a better description of the boundary layer. Vorticity contours of the flow around the cylinders and force time histories are presented. The calculations are also compared to the experimental results obtained by Bearman & Wadcock in 1973 and Williamson in 1985. The numerical simulations, in this sense, complement their work with very detailed vorticity calculations and flow visualizations.

1. INTRODUCTION

The flow about groups of cylinders has been the subject of many studies in the past. Flow interference is responsible for several changes in the characteristics of fluid loads when more than one body is placed in a fluid stream. Investigations of the flow around pairs of cylinders can provide a better understanding of the vortex dynamics, pressure distribution and fluid forces, in cases involving more complex arrangements. This paper presents a detailed numerical study of the flow about a pair of cylinders in side-by-side and in tandem configurations.

The main practical application of this investigation is to have a better understanding of the flow around a bundle of risers which links the seabed to the offshore platforms used for oil exploration. These risers are subject to shear and oscillatory flows due to currents and waves, respectively, flows with a very high degree of complexity, with changes of intensity and direction the deeper the water depth. Most of the Brazilian floating platforms are installed along the continental shelf of the Atlantic Ocean where water depths over 1000 m are common. In such conditions a better understanding of the vortex dynamics causing vibration of risers is essential.

Zdravkovich (1977, 1987) has reviewed the problem of flow interference when two cylinders are placed in side-by-side, tandem and staggered arrangements in a steady current.

0889–9746/01/020327 + 24 $35.00/0

Quoting his words, he observed that "when more than one bluff body is placed in a fluid flow, the resulting forces and vortex shedding pattern may be completely different from those found on a single body at the same Reynolds number". A variety of flow patterns, characterized by the behaviour of the wake region, may be discerned as the spacing between two circular cylinders is changed.

Bearman & Wadcock (1973) investigated the effect of interference with two cylinders in a side-by-side arrangement. They measured the pressure distribution around the bodies, and found a repulsive force between the cylinders for a particular range of gap spacing. They justified the appearance of this force as a consequence of a rotation of the resultant force vector due to the presence of the second cylinder. For a very small gap, Bearman & Wadcock observed a marked asymmetry in the flow with the two cylinders experiencing different drags and base pressures. The gap flow acted as a base bleed, and then the drag of the cylinders in combination was less than the sum of the drags of the isolated cylinders.

The evolution of the wakes formed behind a pair of cylinders placed side by side, has also been studied by Williamson (1985). He found that for a certain range of the gap between the cylinders, the wakes were synchronized, either in phase or in anti-phase. He observed that below a critical gap between the cylinders the flow became asymmetric, similar to the result found by Bearman & Wadcock. Other experimental studies to be mentioned are those by Arie *et al.* (1983), Kim & Durbin (1988) and Summer *et al.* (1998).

Ng & Ko (1995) investigated the problem numerically by using a discrete vortex method. They studied two cylinders in a tandem configuration. In their method two vortices were shed per cylinder in each time step. These vortices were released from the separation points, whose locations were evaluated following the solution of the boundary layer employing the Thwaites' method. The number of vortices was kept below 2000 by the use of an amalgamation procedure. Although the method was very simple, some of the wakes obtained were in very close agreement with experimental results. Mittal *et al.* (1997) studied the case of two cylinders in tandem and in an oblique configuration. The investigation was primarily concerned with the change in the drag coefficient for each of these cases. The main result observed was that the downstream cylinder experienced an increase in drag when it was placed at an oblique configuration. Other numerical studies to be cited are those by Slaouti & Stansby (1992 & 1993). They employed the discrete vortex method including viscous diffusion, modelled by the random walk method, to study the flow around circular cylinders.

The results with a side-by-side configuration of cylinders with the same diameter (D) obtained by Bearman & Wadcock (1973), Williamson (1985) and Kim & Durbin (1988) show that, when the distance (L) between the centres of cylinders is below about $2{\cdot}2D$, only one wake is formed. This wake is deflected in the direction of one of the cylinders in an alternating way. This phenomenon has been named "flopping" or "flip-flopping" by Williamson. The time scale of this flopping is more than 1000 times the time scale of vortex shedding.

When the two cylinders are placed apart in a side-by-side configuration by a distance greater than $2{\cdot}2D$, two wakes are formed and these wakes are most of the time in anti-phase. This has been observed by Williamson and corroborated by Summer *et al.* (1998). For $L > 5D$, the flow around of the cylinders is similar to that encountered for a single circular cylinder.

Three possible regimes are found with two circular cylinders in a tandem arrangement, following Zdravkovich (1977, 1987). The first is observed when the distance between the centres of the cylinders is less than $1{\cdot}2D$–$1{\cdot}8D$ (depending on the Reynolds number). In this case the separating flow from the upstream cylinder is not captured by the wall of the downstream body. In this way, there is the formation of only one wake due to the separating

shear layers from the upstream cylinder. In the second regime, observed for gaps in the range of $1{\cdot}2–1{\cdot}8 < L/D < 3{\cdot}4–3{\cdot}8$, a separation bubble is formed behind the upstream cylinder. It is captured by the downstream body and there is a reattachment of the shear layers emanating from the first cylinder to the wall of the second one. The wake is formed behind the downstream body due to separation occurring on its surface. Finally, in the third regime, for gaps $L/D > 4{\cdot}0$, vortex shedding occurs from both cylinders. The wake behind the second cylinder is called binary, because each vortex is formed by the combination of one vortex shed from the upstream body and another by the downstream cylinder. In the first two regimes, the drag coefficient on the downstream cylinder is considerably lower than the one on the other body. This fact can be understood by noticing that for this case the downstream cylinder is inside the wake formed by the upstream cylinder, i.e., it is immersed in a region of low pressure. This force can even be negative.

It is already known that vortex shedding is a three-dimensional phenomenon. However, two-dimensional simulations at low Reynolds number, as a first approximation to the problem, can be used to give some insight about the details of the vortex dynamics in the wake and vortex impingement occurring when the cylinders are arranged in a tandem configuration. Very few numerical studies about this subject can be found in the literature. The attraction of applying numerical methods to such problems is that the flow can be studied in closer detail. In this sense, fundamental knowledge can be achieved by performing a parametric analysis of the phenomenon in a relatively fast way via the numerical calculations. Most of the calculations in this paper are carried out at a Reynolds number, $\mathrm{Re} = 200$. At this value, the Strouhal number (St) is approximately 0·2. Increasing Re in the pre-critical regime ($200 \leq \mathrm{Re} \leq 10^5 - 5 \times 10^5$), the observed value of St is still close to 0·2, which suggests a certain similarity of the vortex dynamics in this range of Re. This observation enables us to compare, as a first approximation, numerical simulations at low Re with experiments at higher Re, as long as both are in this regime.

This paper is organized as follows: details about the numerical method used in the simulations and the force calculation are presented in the first two sections. The validation of the algorithm follows in the next section. Of the many possible arrangements that two cylinders can be positioned relatively to a cross flow, we have selected two in this investigation. The first group consists of two cylinders in a tandem arrangement, one behind the other at some longitudinal spacing. The second group comprises a pair of cylinders facing the flow in a side-by-side manner. In the third section of this paper, we present the results for these arrangements. Flow visualizations, force time histories, Strouhal number evaluations, are shown for various values of gaps. We also investigate the so-called "flopping" phenomenon and present a FFT analysis of the lift coefficient. In the final section, conclusions are drawn.

2. THEORY AND NUMERICAL METHOD

2.1. Fundamentals of the Method

An explicit computational method is developed in order to investigate the flow around two circular cylinders. A *Fractional Step Method* with Galerkin's finite-element formulation is employed on an unstructured mesh, and a velocity correction projection method is used to solve the Navier–Stokes equations.

The fractional step method with a weighted residual Galerkin formulation shown here is slightly different from the classical *Streamline Upwind Petrov-Galerkin* (SUPG) developed by Brooks & Hughes (1982). In the method presented, which employs the standard Galerkin formulation of the finite-element method, the test functions are the same as trial functions.

One of the attractive properties of this approach is that the discretization of a Laplacian operator results in a symmetric stiffness matrix; in addition, the implementation of homogeneous Neumann's-type boundary conditions is particularly straightforward. In the latter case, both weighting and interpolation functions are not selected from the same class of functions. Instead, the Galerkin weighting functions are replaced by the so-called Hughes weighting functions, leading to a variational formulation which differs from the Galerkin method, so that some of the terms are multiplied by the Petrov–Galerkin functions.

Following Manna (1997), the fractional step concept is considered a generic approach and several variations can be found in the literature. The particular method shown here has also been developed by Meling & Dalheim (1997). The governing equations for a Newtonian, incompressible viscous flow are the conservation of mass and the Navier–Stokes equations. In two-dimensions and without body forces, they may be written as follows:

$$\frac{\partial u_i}{\partial x_i} = 0, \quad i = 1, 2, \tag{1}$$

$$\frac{\partial u_i}{\partial t} + u_j \frac{\partial u_i}{\partial x_j} = -\frac{1}{\rho}\frac{\partial p}{\partial x_i} + \nu \frac{\partial^2 u_i}{\partial x_j \partial x_j}, \tag{2}$$

where the summation convention applies, u_i are the velocity components, p is the pressure, ν is the kinematic viscosity, and ρ is the density of the fluid. The outer boundary condition for the velocity is its free-stream value and for the pressure is a prescribed value equal to P_∞. On the circular cylinder surface a no-slip condition is applied, which implies that the fluid velocity is zero.

A fractional step formulation is applied for the time discretization of the governing equations (1) and (2). First, an intermediate velocity is computed by neglecting the pressure. The pressure field is then calculated by means of a Poisson's equation, and the velocity field is finally corrected by including the pressure effect. For the purpose of determining a intermediate velocity a two-step Taylor–Galerkin formulation is employed.

Considering a time increment $\Delta t = t^{(n+1)} - t^{(n)}$, the fractional step method algorithm is given as follows:

(i) at time $t^{(n+1)}$ an intermediate velocity $\tilde{u}_i$ is calculated by means of an integration of the reduced momentum equation omitting the pressure:

$$\tilde{u}_i^{(n+1)} = u_i^{(n)} - \int_{t_n}^{t_n+1} \left[u_j \frac{\partial u_i}{\partial x_j} - \nu \frac{\partial^2 u_i}{\partial x_j \partial x_j} \right] dt, \quad i, j = 1, 2; \tag{3}$$

(ii) the complete velocity u_i at $t^{(n+1)}$ is computed by including the pressure field:

$$u_i^{(n+1)} = \tilde{u}_i^{(n+1)} - \frac{1}{\rho} \int_{t_n}^{t_n+1} \frac{\partial p}{\partial x_i} \, \mathrm{d}t; \tag{4}$$

(iii) the final velocity field must satisfy the continuity equation, i.e.

$$\left(\frac{\partial u_i}{\partial x_i} \right)^{n+1} = 0. \tag{5}$$

In order to solve the first step of this algorithm, a predictor–corrector formulation, as suggested by Meling & Dalheim (1997), is employed. An intermediate velocity $\tilde{u}_i^{(n+1/2)}$, at a time increment $\Delta t/2$, is calculated, and then the velocity $u_i^{(n)}$ is up-dated

as follows:

$$\tilde{u}_i^{(n+1/2)} = u_i^{(n)} - \frac{\Delta t}{2}(u_j)^{(n)}\left(\frac{\partial u_i}{\partial x_j}\right)^n, \tag{6}$$

$$\tilde{u}_i^{(n+1)} = u_i^{(n)} - \Delta t\left[(u_j)^n\left(\frac{\partial \tilde{u}_i}{\partial x_j}\right)^{n+1/2} - \nu\left(\frac{\partial^2 u_i}{\partial x_j \partial x_j}\right)^n\right]. \tag{7}$$

The velocity evaluated by equation (7) is employed for the convection in the correction step of the method.

The second and third steps are responsible for the computation of the complete velocity field that satisfies the continuity equation and they are combined by means of a pressure equation (Poisson's equation). Taking the divergence of the following discretized form of equation (4)

$$u_i^{(n+1)} = \tilde{u}_i^{(n+1)} - \frac{\Delta t}{\rho}\left(\frac{\partial p}{\partial x_i}\right)^{n+1} \tag{8}$$

and using the continuity equation given in equation (6), the Poisson's equation that arises is given by

$$\frac{\Delta t}{\rho}\left(\frac{\partial^2 p}{\partial x_j \partial x_j}\right)^{n+1} = \left(\frac{\partial \tilde{u}_j}{\partial x_j}\right)^{n+1}. \tag{9}$$

An alternative form of the algorithm could include the known pressure field for the prediction of the intermediate velocity, and then computing the pressure difference instead of including the complete pressure field. However, as can be seen in Meling & Dalheim (1997), the removal of the pressure term in equation (3) has advantages, since no spurious pressure modes are obtained. An equal order of interpolation can still be used for velocity and pressure. In the case of the standard SUPG, there is no inclusion of pressure stabilization, and the pressure interpolation functions remain unchanged.

As far as the Babuska–Brezzi stability criterion is concerned, the inf–sup test (Brezzi & Fortin 1991) has not been checked in this work rigorously (numerically). Nevertheless, the authors were aware about the boundary conditions, at least assuming them smooth. In this way, as can be seen later on this paper, the extension of the outer boundary has been set in order not to cause any perturbation in the near-wake flow.

Regarding the boundary conditions for the complete velocity field, the prescribed values considered for the cylinder wall and outer boundary conditions have also been set for the intermediate step. According to the authors' experience, also observed in three-dimensional studies [see Siqueira *et al.* (2000)], this procedure does not give rise to unrealistic or doubtful solutions.

2.2. Finite-Element Formulation for the Spatial Discretization

A Galerkin finite-element formulation is applied to the spatial discretization of the algorithm described previously for an unstructured three-noded mesh. As can be seen in Zienkiewicz & Morgan (1983), for any two-dimensional analysis the triangle is a particularly useful shape and can represent with a high degree of accuracy regions enclosed by boundaries of any shape.

The connectivity between elements and nodes (named as i, j and k) is arranged under the consistent node numbering system of an anticlockwise order. The continuity requirement of

the shape functions can be ensured by assuming a linear form as follows:

$$N_i^e = \alpha_i^e + \beta_i^e x + \gamma_i^e y, \quad i = 1, 2, 3. \tag{10}$$

The constants in this expression are given by

$$\alpha_i^e = \frac{x_j y_k - x_k y_j}{2\Delta^e}, \quad \beta_i^e = \frac{y_j - y_k}{2\Delta^e}, \quad \gamma_i^e = \frac{x_k - x_j}{2\Delta^e}, \tag{11}$$

where Δ^e is the area of the element. Definitions for the other coefficients related to remaining nodes j and k are cyclic rearrangements of the above, leading to similar expressions.

The fields of velocity and pressure are approximated by a piecewise linear spatial variation over the elements in the domain. The representation is therefore

$$u_i \approx \mathbf{N}\mathbf{U}_i, \quad p \approx \mathbf{N}\mathbf{P}, \tag{12}$$

where $\mathbf{N}$ is the shape function vector, $\mathbf{U}_i$ and $\mathbf{P}$ represent the nodal values of the velocity components and pressure, respectively.

Applying a weighted residual formulation to the governing equations, one obtains the following set of matrix equations:

$$\mathbf{C}^n \tilde{\mathbf{U}}_i^{n+1/2} = \mathbf{C}^n \mathbf{U}_i^n - \frac{\Delta t}{2} \mathbf{A}^n \mathbf{U}_i^n, \tag{13}$$

$$\mathbf{C}^n \tilde{\mathbf{U}}_i^{n+1} = \mathbf{C}^n \mathbf{U}_i^n - \Delta t [\mathbf{A}^n \tilde{\mathbf{U}}_i^{n+1/2} + \nu \mathbf{K}^n \mathbf{U}_i^n], \tag{14}$$

$$\mathbf{K}^n \mathbf{P}^{n+1} = -\rho \mathbf{D}_j^n \tilde{\mathbf{U}}_j^{n+1}, \tag{15}$$

$$\mathbf{C}^n \mathbf{U}_i^{n+1} = \mathbf{C}^n \tilde{\mathbf{U}}_i^{n+1} - \Delta t \frac{1}{\rho} \mathbf{D}_i^n \mathbf{P}^{n+1}, \tag{16}$$

where the boundary integrals resulting from integration by parts of the diffusion term and the pressure Poisson equation are omitted due to the applied boundary conditions.

The global matrices are then defined as follows:

$$\mathbf{C}^n = \int_{\Omega^n} \mathbf{N}^{\mathrm{T}} \mathbf{N} \, \mathrm{d}\Omega, \qquad \mathbf{A}^n = \sum_{e=1}^{n} (\bar{C}_j)_e \int_{\Omega_e^n} \mathbf{N}^{\mathrm{T}} \frac{\partial \mathbf{N}}{\partial x_j} \, \mathrm{d}\Omega, \tag{17, 18}$$

$$\mathbf{D}_j^n = \int_{\Omega^n} \mathbf{N}^{\mathrm{T}} \frac{\partial \mathbf{N}}{\partial x_j} \, \mathrm{d}\Omega, \qquad \mathbf{K}^n = \int_{\Omega^n} \frac{\partial \mathbf{N}^{\mathrm{T}}}{\partial x_j} \frac{\partial \mathbf{N}}{\partial x_j} \, \mathrm{d}\Omega, \tag{19, 20}$$

where $(\bar{C}_j)_e$ is the element mean convective velocity component, evaluated at the element centroid. This "centroid convection velocity" procedure was first proposed by Gresho *et al.* (1984) and simplifies the convection matrix.

Rather than loop over the elements whilst calculating the local element stiffness matrix, the global matrices are assembled prior to the time march. The stiffness matrix is a discretization of the Laplacian, and since it is a symmetric matrix, only the upper triangular part is stored, in order to save memory. Because the mesh is fully unstructured, the global matrices have no structure, and are stored in a format which puts subsequent nonzeros in contiguous memory locations. These are assembled in a pre-processing program.

The preceding linear systems that should be solved in the present method require an efficient, fast and accurate solver for sparse, symmetric and banded matrices. The preconditioned conjugate gradient method with diagonal scaling was implemented in this work for this purpose.

Following Barrett *et al.* (1992), the convergence rate of iterative methods depends on spectral properties of the coefficient matrix. The purpose of using a preconditioner is an attempt to transform the linear system into one that should be equivalent and has more favourable spectral properties. In this paper the diagonal scaling was employed, which improved convergence rates dramatically. This was suggested by Arkell (1997) in a private communication and consists of taking as preconditioner the diagonal of the coefficient matrix.

2.3. Force Evaluation

Force coefficients are calculated by suitably integrating the pressure and skin friction contributions. The pressure distribution around the surface of the cylinder is obtained from the solution of the Poisson's equation for the pressure, i.e., the solution of equation (13). The skin friction contribution is obtained from the definition of the shear stress at the wall, which yields

$$\tau_{\text{wall}} = -\mu \frac{\partial u_t}{\partial n}, \tag{21}$$

where μ is the dynamic viscosity, τ_{wall} is the shear stress, u_t is the tangential velocity at the wall, and n is the normal direction to the wall. After considering the contributions from skin friction and pressure, the force components are resolved in the two directions (x, y), yielding F_x and F_y. These forces are then nondimensionalized as follows:

$$C_l = \frac{2F_y}{\rho U_\infty^2 D}, \qquad C_d = \frac{2F_x}{\rho U_\infty^2 D}, \tag{22, 23}$$

where ρ is the fluid density, and U_∞ is the free-stream velocity.

3. NUMERICAL RESULTS

3.1. Validation of the Algorithm

In order to validate the computational code, two-dimensional simulations in a Reynolds number range varying from 100 to 200 have been carried out. The Reynolds number is defined in terms of the cylinder diameter (D) and the free stream velocity (U), $\text{Re} = \text{UD}/\nu$. A nondimensional time step, Ut/D, equal to 0·0050 has been used.

An unstructured finite element mesh with 27 062 elements and 13 696 nodes has been used. This mesh can be seen in Figure 1 and details near the cylinder surface are shown in Figure 2. There are 128 points in order to discretize the cylinder wall. The centre of the cylinder is located at co-ordinate (0,0). The extension of the outer boundary has been set in order not to cause any perturbation in the near-wake flow. The first node near the cylinder wall is located at a distance of about 1% of the cylinder radius. Ten nodes are positioned within a sub-domain delimited by a normal distance of $0{\cdot}15D$ from the cylinder wall. Tests have been performed indicating that the mesh with this definition lead to a suitable boundary layer discretization. Other sub-domains are created for the wake and for the fair-field regions as shown in Figures 1 and 2. These latter regions are then filled with triangles using the program ANSYS 5.1. During the generation process, ANSYS meshing algorithms automatically generate elements using mesh smoothing and enhancement procedures, which prevent from creating poorly shaped elements.

Primarily, comparisons of the drag coefficient and Strouhal number for a single cylinder at various values of Reynolds (Re) number were carried out and the results compared to

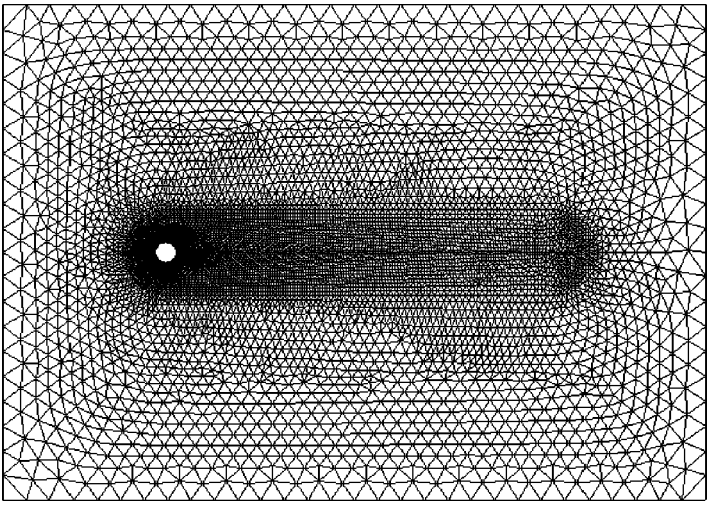

Figure 1. Unstructured finite-element mesh for a single cylinder.

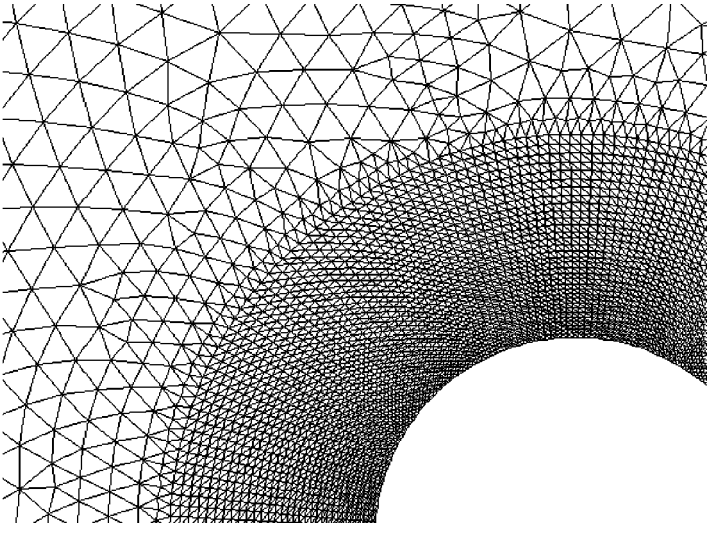

Figure 2. Details of the mesh used in the boundary layer.

published data to validate the computational method. The Strouhal number is defined in terms of the cylinder diameter (D), the free-stream velocity (U), and the frequency (n) of oscillation of the lift coefficient, $\mathrm{St} = nD/U$. In Table 1, the results for $\mathrm{Re} = 100$ are presented and compared with results from other simulations and experiments. The average drag coefficient is 1·37, which is the same as the one found in the numerical simulations by Braza *et al.* (1986), and slightly lower than the one found by Meneghini (1993) using a hybrid discrete vortex method. The Strouhal number found in the present simulation is very close to the experimental result obtained by Williamson (1991), as can be seen in Table 1.

TABLE 1
Average drag coefficients and Strouhal numbers for a single cylinder at Re = 100. Comparison with literature data

	St (Strouhal number)	$C_{d_{av}}$ (average drag coefficient)
Current fractional step method	0·165	1·37
Other results found in the literature		
Braza *et al.* (1986)	0·160	1·37
Sa & Chang (1991)	0·155	1·23
Meneghini (1993)	0·162	1·52
Saltara (1999)	0·160	1·33
Experiments		
Roshko (1954)	0·16–0·17	
Tritton (1959)		1·25
Williamson (1991)	0·164	

TABLE 2
Average drag coefficients and Strouhal numbers for a single cylinder at Re = 200. Comparison with literature data

	St	$C_{d_{av}}$
Current fractional step method	0·196	1·30
Other results found in the literature		
Borthwick (1986)	0·188	1·02
Braza *et al.* (1986)	0·200	1·35
Sa & Chang (1991)	0·186	1·13
Meneghini (1993)	0·196	1·25
Arkell (1995)	0·196	1·30
Giannakidis (1997)	0·190	1·25
Saltara (1999)	0·190	1·25
Experiments		
Roshko (1954)	0·17–0·19	
Williamson (1991)	0·196	
Norberg (1993)		1·30

The results for Reynolds number equal to 200 are summarized and compared to other calculations and experiments in Table 2. For this Re the Strouhal number obtained here, i.e. St = 0·196, is the same as the value obtained by Meneghini (1993), Arkell (1995) and Giannakidis (1997). All these calculations compare very well with the experimental result obtained by Williamson. The average value of drag coefficient is 1·30, comparing very well with the one obtained experimentally by Norberg (1993) and other literature data for this Reynolds number, as can be seen in Table 1. The peak-to-peak value of the lift is 1·40. The wake structure, represented by the streaklines, is given in Figure 3. Lift and drag coefficient time histories are shown in Figure 4.

It is interesting to see the comparison of the Strouhal number curve obtained with the simulations and the one obtained by Williamson in his experiments with very controlled experimental conditions. This curve is shown in Figure 5, together with results obtained by other simulations. The agreement here also is very good, showing the applicability of the present algorithm to study vortex shedding from circular cylinders.

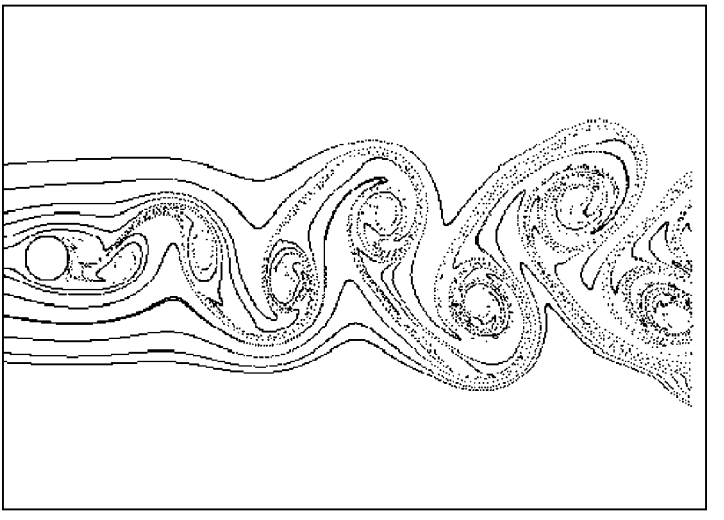

Figure 3. Wake structure for a single circular cylinder for Re = 200.

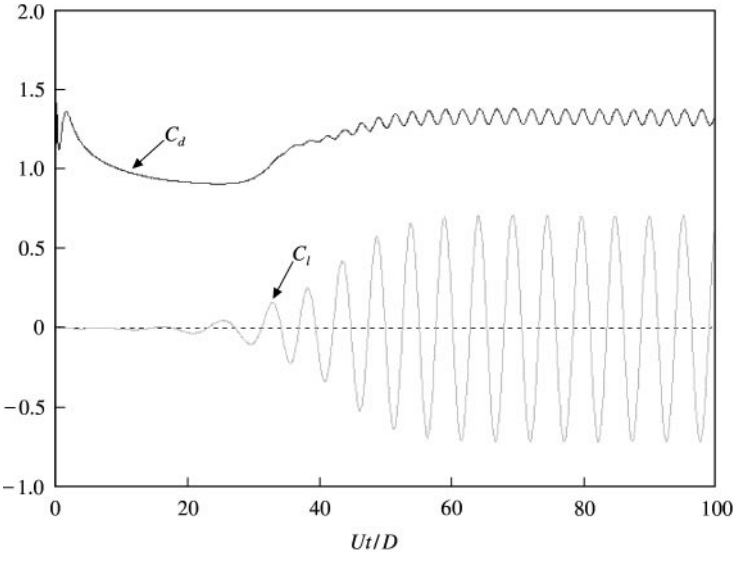

Figure 4. Force coefficients for Re = 200, single cylinder.

3.2. Tandem Arrangements

In order to investigate the proximity effect on vortex shedding, simulations have been carried out for cylinders in tandem and side-by-side arrangements. For both cases, the gap (L) between the centres of the cylinders, which have the same diameter, was chosen in range $1{\cdot}5D < L < 4D$. A typical computational unstructured finite-element mesh for the tandem arrangement is shown in Figure 6. The mesh shown refers to a gap of $3D$ and consists of 26 064 elements and 13 219 nodes. Table 3 gives the nodal density of the meshes for the case where the gap is $L = 1{\cdot}5D$ and $4D$ for both tandem and side-by-side arrangements, showing the range of variation in the number of elements and nodes for our study. The CPU time in each case for a completion of a total nondimensional time of 500 is given in Table 4. All the

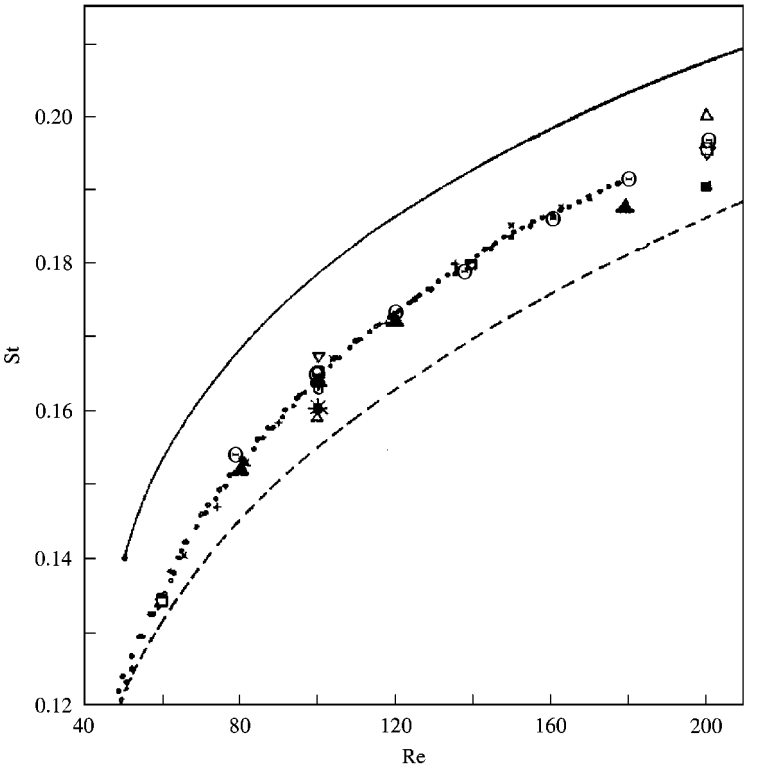

Figure 5. Comparison between experimental and numerical results (Fractional Step Method). Extended from Williamson (1991): *Experimental results*: ●, wind tunnel, parallel shedding; ○, wind tunnel, oblique shedding; ×, water tank; +, water tank. *Numerical results*: —, Karniadakis & Triantafyllou (1989); – – – –, Sa & Chang (1991); △, Braza *et al.* (1986); □, Lecointe & Piquet (1988); ■, Martinez (1979); ▽, Koschel *et al.* (1989); ⋆, Young & Ni (1989); ∗, Dolan *et al.* (1990); ▲, Shariff *et al* (1990); Θ, present simulation.

simulations were performed in an AlphaServer DS 20, dual processor (Alpha EV6 500 MHz) with 1 gbyte of memory.

The Reynolds number for all the simulations is equal to 200. The radius (R) of the cylinders is equal to 1 and the point with coordinate (0,0) is located at the middle distance between the cylinders. The outer boundary of the mesh extends downstream to $50R$ and upstream to $21{\cdot}3R$. In the vertical direction, the outer boundaries are located at $-21{\cdot}3R$ and $21{\cdot}3R$.

The nondimensional time step, $U_0\Delta t/D$, is set to 0·005. The closest mesh point in the normal direction to the wall is located at a distance of around $0{\cdot}01R$, and the mesh point distribution is concentrated near the wall in order to give a very accurate boundary-layer solution. Figure 7 shows a detailed view of the mesh near the wall of both cylinders, stressing the importance of a suitably concentrated nodal distribution in the boundary layer region. The number of nodes and triangles used for the simulations for the other gap values is slightly different, however, the general characteristics of the meshes are very similar.

Force coefficient time histories for the gap values simulated are shown in Figure 8. The drag coefficient is positive for the upstream cylinder and negative for the downstream cylinder for gaps less than $3D$. The net effect of these drag, values is the manifestation of an

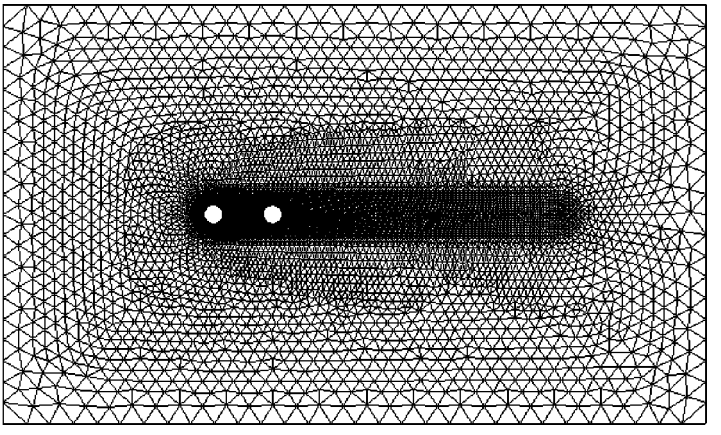

Figure 6. Typical unstructured finite element for the tandem arrangement. Distance between the centres equal to $3D$.

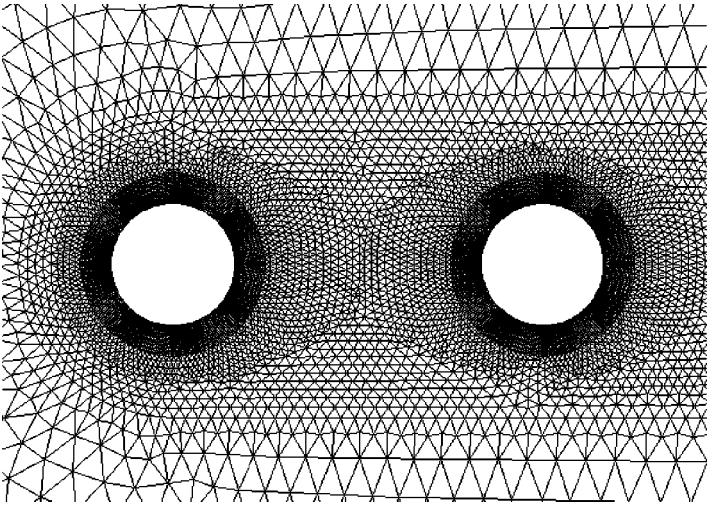

Figure 7. Detail of the mesh near the wall for both cylinders. Distance between the centres equal to $3D$.

attraction force between the cylinders. The drag coefficient on the downstream cylinder turns out to be less negative as the gap increases. These results are in accordance with the experimental observations by Zdravkovich (1987), in which a negative drag has been observed for the same gap range. The simulations were carried out from an impulsive starting flow to $Ut/D = 400$.

The lift coefficient time histories shown in panels (ii) and (iv) of Figures 8(a) and 8(b), for gap values of $L = 1{\cdot}5D$ and $2D$, respectively, depict a small amplitude for both cylinders. It is interesting to note that for $L = 2D$ it takes many cycles for the flow to settle down and reach a steady condition in terms of vortex shedding. As the gap is increased to $3D$, the amplitude of the lift on the downstream body reaches the order of magnitude observed in the case of an isolated cylinder. The lift on the upstream cylinder still has a low amplitude for this value of gap.

When the gap is increased from $3D$ to $4D$, a very distinct change in the flow characteristics occurs. The upstream cylinder starts to shed vortices. For $L = 4D$, the lift coefficients of

TABLE 3
Nodal density for $L = 1{\cdot}5D$ and $4D$. Tandem and side-by-side arrangements

Value of Gap L	Arrangement	Number of elements	Number of nodes
$1{\cdot}5D$	Tandem	24 770	12 562
$4D$	Tandem	26 300	13 327
$1{\cdot}5D$	Side-by-side	27 284	13 819
$4D$	Side-by-side	30 896	15 645

TABLE 4
CPU time for the completion of a total non-dimensional time of 500

Value of Gap L	Arrangement	CPU time
$1{\cdot}5D$	Tandem	1 h 10 min
$4D$	Tandem	1 h 25 min
$1{\cdot}5D$	Side-by-Side	1 h 34 min
$4D$	Side-by-side	1 h 46 min

both cylinders oscillate, with the highest amplitude experienced by the downstream body. The drag of this cylinder becomes positive, even though with an intensity considerably lower than the one from the upstream body. The drag on the upstream cylinder increases from about 1·0 to approximately 1·2. If the gap is further enlarged, the drag on both cylinders increases, suggesting that at higher gaps the result of the drag from an isolated cylinder may be recovered.

The streaklines and vorticity contours shown in Figures 9 and 10 give a very interesting picture of the flow condition for each case. The plots in these figures are at $Ut/D = 200$. The wakes are represented by the respective streaklines. The vorticity contours are nondimensionalized by the cylinder radius and the free-stream velocity. Figure 10(a) and 10(b) depict the vorticity contours for a gap of $1{\cdot}5D$ and $2D$, respectively. Analysing these figures one can see that the cylinders act as a single body, with only one vortex wake forming behind the downstream cylinder. The separating shear layer from the upstream cylinders involves the downstream body. The interaction between these shear layers takes place only in the base region of the downstream cylinder, with a consequent vortex formation and shedding occurring behind this body. If one compares the formation distance of an isolated cylinder with the case of the arrangement shown in Figure 10(a), it is clearly perceived that in the former the vortex shedding process occurs much closer to the base of the body. The lift coefficient has small amplitude, as shown in Figure 8(a). When the gap is $2D$, Figure 10(b), the wake forms even further downstream. The lift coefficient for this case does not oscillate with a constant frequency and its amplitude is low compared to the isolated cylinder case.

In Table 5, the drag coefficients and Strouhal numbers of the cases simulated are shown and compared with those of an isolated cylinder. The numbered index in the coefficients refers to the upstream cylinder (index 1) and the downstream cylinder (index 2). For gaps in the range $1{\cdot}5D < L < 3D$ the drag varies from $-0{\cdot}18$ to $-0{\cdot}08$, indicating that the downstream cylinder is immersed on a low-pressure region formed by the separated shear

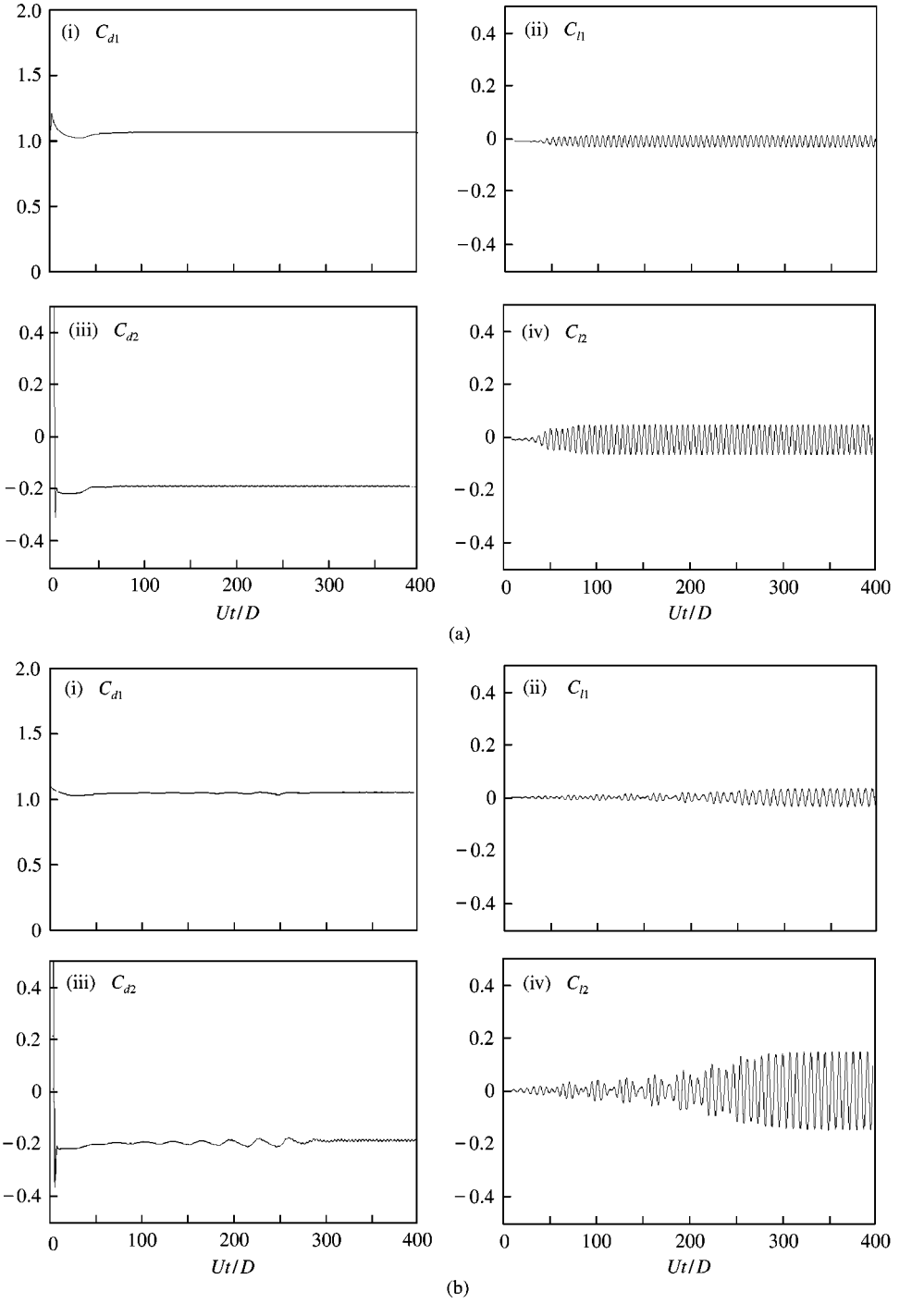

Figure 8. Force coefficients time history, tandem arrangement (Re = 200). Distance between the centres (a) $L = 1.5D$, (b) $2D$, (c) $3D$, and (d) $4D$. C_d is the drag coefficient and C_l is the lift coefficient. Index 1 refers to the upstream circular cylinder, and index 2 to the downstream circular cylinder.

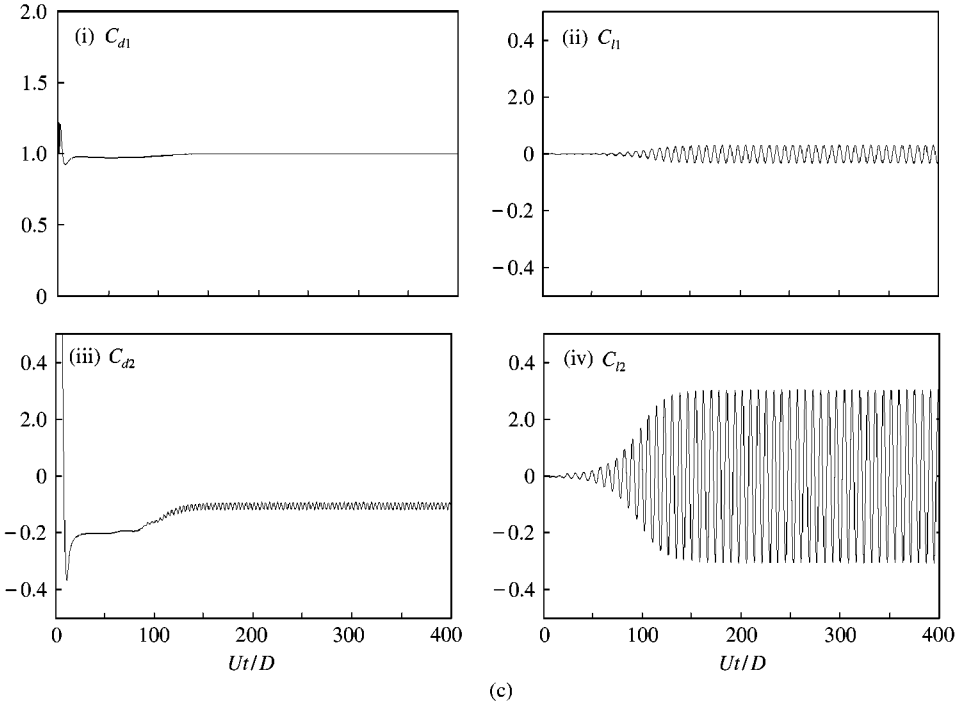

(c)

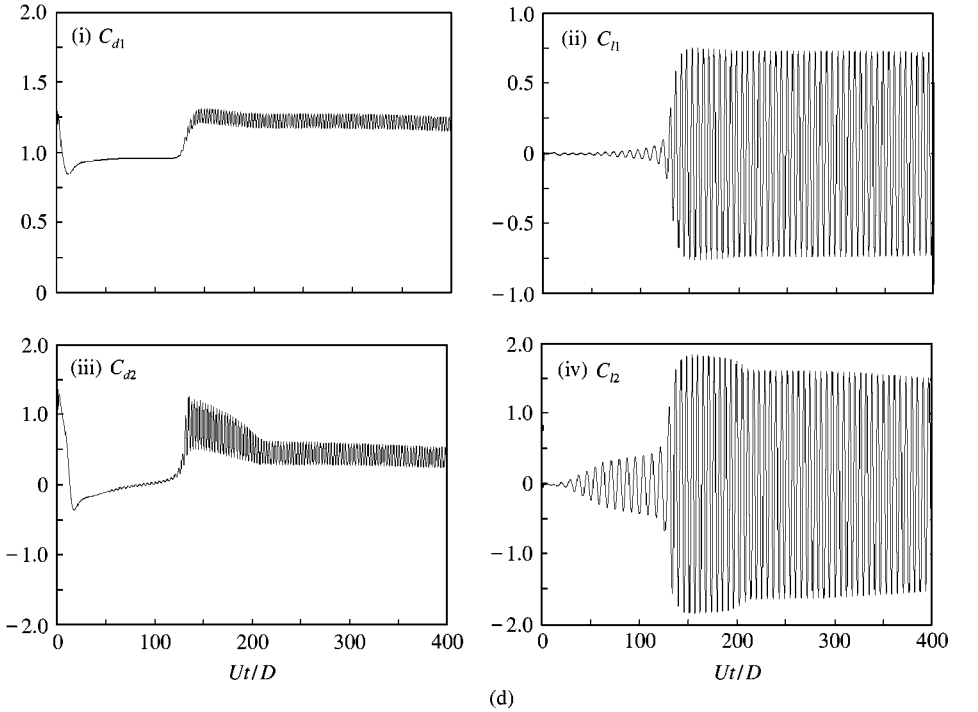

(d)

Fig. 8. (*continued.*)

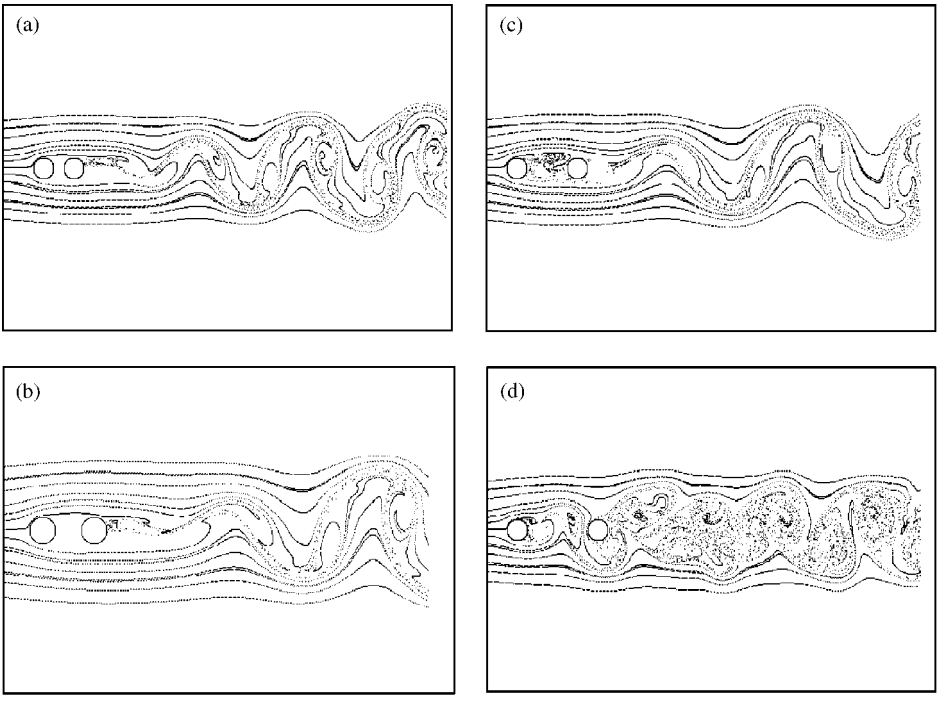

Figure 9. Wake structure represented by streaklines, tandem arrangement (Re = 200). (a) $L = 1{\cdot}5D$, (b) $2D$, (c) $3D$, and (d) $4D$.

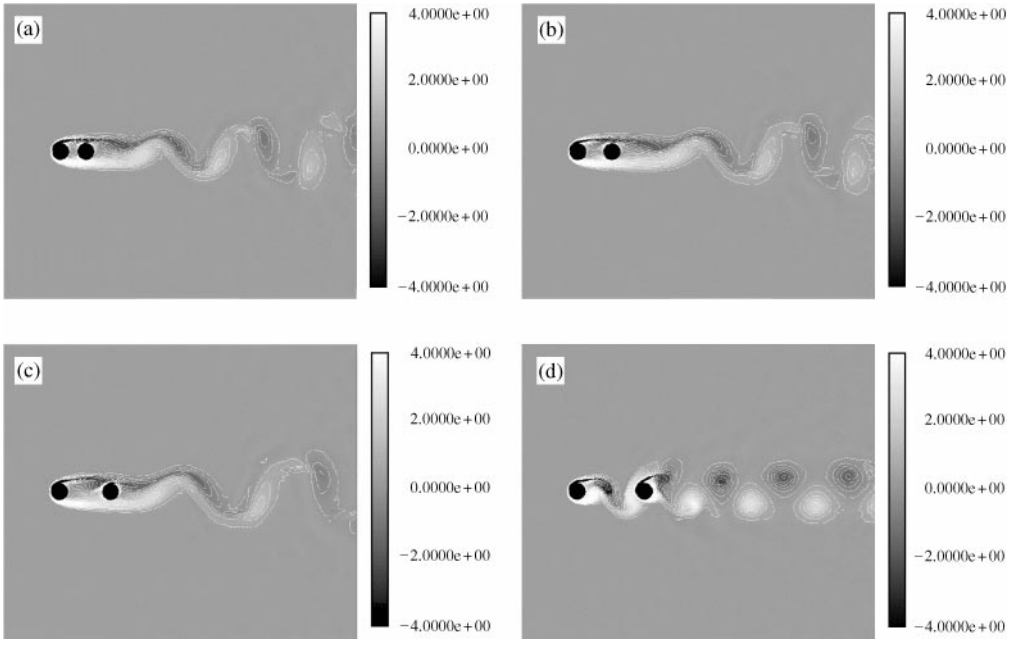

Figure 10. Vorticity contours, tandem arrangement (Re = 200). (a) $L = 1{\cdot}5D$, (b) $2D$, (c) $3D$, and (d) $4D$.

TABLE 5
Average drag coefficient and Strouhal number for the tandem configuration, index 1 refers to the upstream cylinder and index 2 to the downstream cylinder

Gap	$C_{d_{m1}}$	$C_{d_{m1}}/C_d$	$C_{d_{m2}}$	$C_{d_{m2}}/C_d$	St_1	St_2
1·5D	1·06	0·815	−0·18	−0·139	0·167	0·167
2D	1·03	0·792	−0·17	−0·131	0·130	0·130
3D	1·0	0·770	−0·08	−0·060	0·125	0·125
4D	1·18	0·910	0·38	−0·290	0·174	0·174

layers emanating from the upstream body. The wake visualizations and vorticity contours presented in Figures 9 and 10, respectively, corroborate this conclusion.

It is interesting to mention the change in Strouhal number that occurs due to the interference. For the small gaps, the Strouhal (St) number is considerably lower than the one found in the case of an isolated cylinder. A minimum value of St = 0·127 is reached for a gap $L = 3D$. This value is about 65% of the Strouhal number found in an isolated cylinder (St = 0·196).

3.3. SIDE-BY-SIDE ARRANGEMENTS

Simulations have been carried out with two cylinders in a side-by-side arrangement for gaps in the range $1{\cdot}5D < L < 4D$. As in the case of the pair of cylinders in tandem, the point with coordinates (0,0) is located at the middle distance between the cylinders. The time step, free-stream velocity and Reynolds number are the same as in the previous cases. A typical computational unstructured finite element mesh for the side-by-side arrangement is shown in Figure 11. The example given refers again to $L = 3D$, where L is the distance between the centres of the cylinders. The computational mesh for this case consists of 27 672 elements and 14 013 nodes. Figure 12 shows a detail of the mesh near the cylinder walls, stressing the importance of a suitably concentrated nodal distribution in the boundary layer. The number of triangles and nodes for the cases with other values of L is slightly different, but the characteristics of the meshes are essentially the same. All simulations for the side-by-side arrangement have been carried out until a nondimensional time of 1500. These very long runs were necessary to obtain power spectra of the lift coefficient. However, for the sake of clarity the force coefficient time histories are shown until the nondimensional time of 200 or 400.

In panels (i) of Figure 13(a–d) the time history of the force coefficients for the case $L = 1{\cdot}5D$ can be seen. Pressure contours can be seen in Figure 14(a). For this case there is a repulsive force acting on the cylinders, in accordance with the results observed experimentally by Bearman & Wadcock (1973) and Williamson (1985). In Figure 13(a) is possible to note that the average lift coefficient of the upper cylinder is positive and this coefficient for the lower cylinder is negative. An explanation for this behaviour can be found analysing the pressure contours shown in Figure 14(a). In these contours, high-pressure regions are indicated by a red colour, and negative ones by a blue colour. A region of high-pressure forms in front of the cylinders. A pressure drop occurs as the fluid flows through the gap. However, the pressure along this interstitial region (indicated by a transition from a yellowish colour to a light-blue colour) is still higher than the pressure at both opposite sides of the cylinders (darker blue colour). The frontal stagnation points move in the direction of the gap. The positions of the separation points in the lower and upper cylinders move clockwise

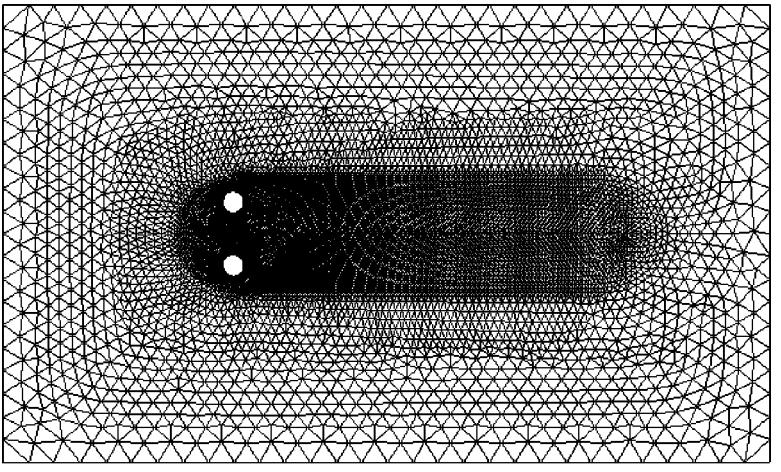

Figure 11. Typical unstructured finite element for the side-by-side arrangement. Distance between the centres equal to 3*D*.

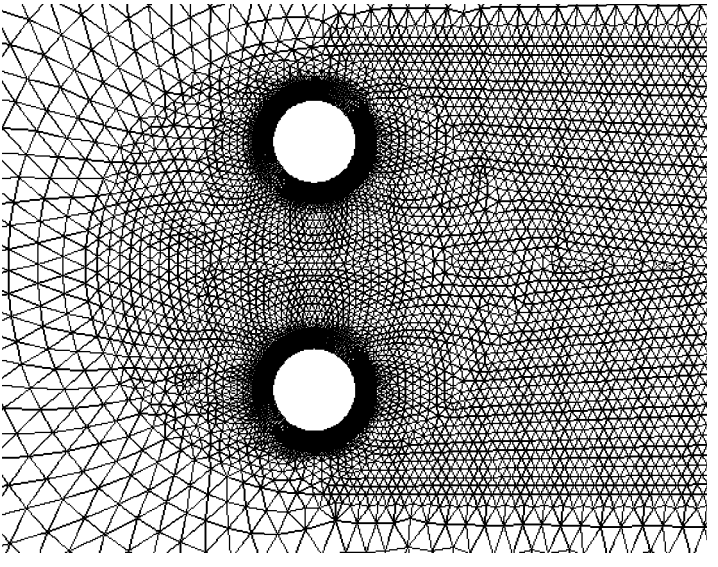

Figure 12. Detail of the mesh near the wall for both cylinders equal to 3*D*.

and anti-clockwise, respectively, compared to the positions of the separation point of an isolated cylinder. The net result of this pressure field is to cause a repulsive force between the cylinders.

The drag coefficient time histories depicted in panels (i) and (iii) Figure 13(a) provides evidence of a "flopping" behaviour of the wake, as described by Kim & Durbin (1988). As the wake is deflected towards one of the cylinders, its drag increases. The wake visualized in Figure 15(a) is similar to the wake formed behind a single body. However, the flopping observed experimentally by Kim & Durbin has a time scale considerably higher than the one observed in the present simulation. They observed that the wake was deflected towards one of the cylinders and it remained deflected during several cycles of vortex shedding.

A possible explanation for this disagreement may be due to the fact that the simulations are two-dimensional and at a lower Reynolds number.

The results for $L = 2{\cdot}0D$ are shown in Figures 13(b) and 15(b). The flopping phenomenon can still be seen in the drag time history. The vorticity contours for this gap are shown in Figure 16(b). The repulsive force between the cylinders is diminished, but the wake still resembles the wake of a single body. For this spacing the wake is clearly not organized, with the time histories of the force coefficients indicating only the net effect of repulsion between the cylinders.

In our simulations for $L = 3{\cdot}0D$, the flopping vanishes. It is possible to observe in Figure 13(c) that the drag coefficients for both cylinders are the same and the lift coefficients are in anti-phase. In Figures 16(c) and 14(c) we can perceive that the wakes are in anti-phase, as observed experimentally by Bearman & Wadcock (1973) and Williamson (1985). The wakes behind each cylinder are antisymmetrical. As the gap increases, there is a synchronization of the lift from the upper and lower cylinders with a phase of about 180°, corroborating the anti-phase wake visualization. This behaviour is also observed for a gap $L = 4{\cdot}0D$, as can be seen in Figure 13(d). For higher values of the gap, the repulsion force between the cylinders diminishes, suggesting that the isolated cylinder result is recovered.

Fourier analysis of the lift coefficient on the upper cylinder, for the cases of gaps $L = 1{\cdot}5D$, $2D$ and $3D$, is shown in Figure 17. In this figure, the abscissa represents the nondimensional frequency ($\bar{f}$) and the power-spectrum estimation is shown in a log scale. It is interesting to notice that for the cases where the gap is $1{\cdot}5D$ and $2D$ the spectra are broad-banded with a peak, not particularly sharp, located at $\bar{f} \simeq 0{\cdot}2$, i.e., the Strouhal frequency. For these gaps the "flopping" phenomenon has been observed and the wakes are not synchronized. The characteristics of the spectra observed are in agreement with the random nature of the lift results shown in Figure 13(a) and 13(b).

As the gap is increased to $L = 3D$, the wakes forming from the two cylinders become synchronized, and the spectrum presented in Figure 17(c) shows a very distinctive peak at $\bar{f} \simeq 0{\cdot}2$. For this case there are other peaks at the two sub-harmonics, $\bar{f} \simeq 0{\cdot}4$ and $0{\cdot}6$.

The average drag coefficient results for the values of gap simulated here are shown in Table 6. These drag coefficients are compared with the one from an isolated cylinder. Analysing this table, it is possible to see that as the gap increases, the ratio between the drag on either cylinder and the drag on an isolated cylinder begins to fall, and would eventually tend to 1·0. The highest drag amplifications occurred for gaps $L = 2{\cdot}0D$ and $3{\cdot}0D$, where there was an increase of about 9 and 8%, respectively.

4. CONCLUDING REMARKS

In this work, a computational algorithm has been developed and used for the calculation of the flow around two cylinders in tandem and side-by-side arrangements, for $\mathrm{Re} = 200$. Vorticity contours and force coefficient time histories were presented. For the tandem arrangement, the results were similar to those observed in the experiments. A negative drag force on the downstream cylinder was observed for gaps less than $3D$ and a positive drag force for gaps above $3D$. For values of $L < 3D$ vortices are shed only from the downstream cylinder and for values of $L \geq 3D$ vortices are shed from both bodies. In this case, vortices hit the downstream cylinder and they undergo an amalgamation process with the vortices forming and being shed from the second body.

For the side-by-side arrangement, a repulsion force between the cylinders has been observed for gaps $L \leq 2D$, similar to the experimental results obtained by Bearman & Wadcock (1973) and Williamson (1985). The analysis of the pressure contours for this case gave an explanation for this behaviour. Also, a "flopping" phenomenon has been

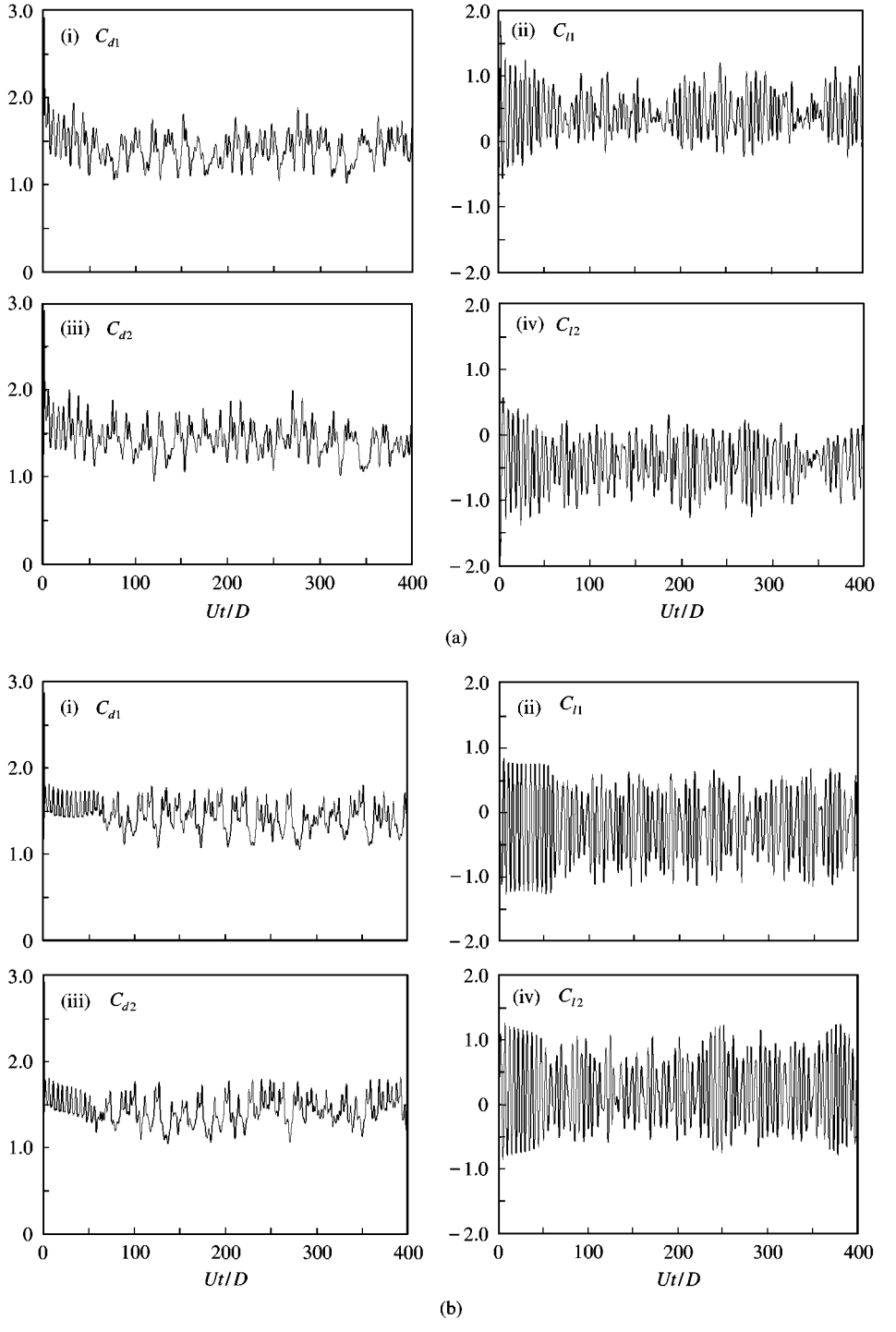

Figure 13. Force coefficients against nondimensional time. Side-by-side arrangement (Re = 200). (a) $L = 1{\cdot}5D$, (b) $2D$, (c) $3D$, and (d) $4D$. C_d is the drag coefficient and C_l is the lift coefficient. Index 1 refers to the upper circular cylinder and index 2 to the lower circular cylinder.

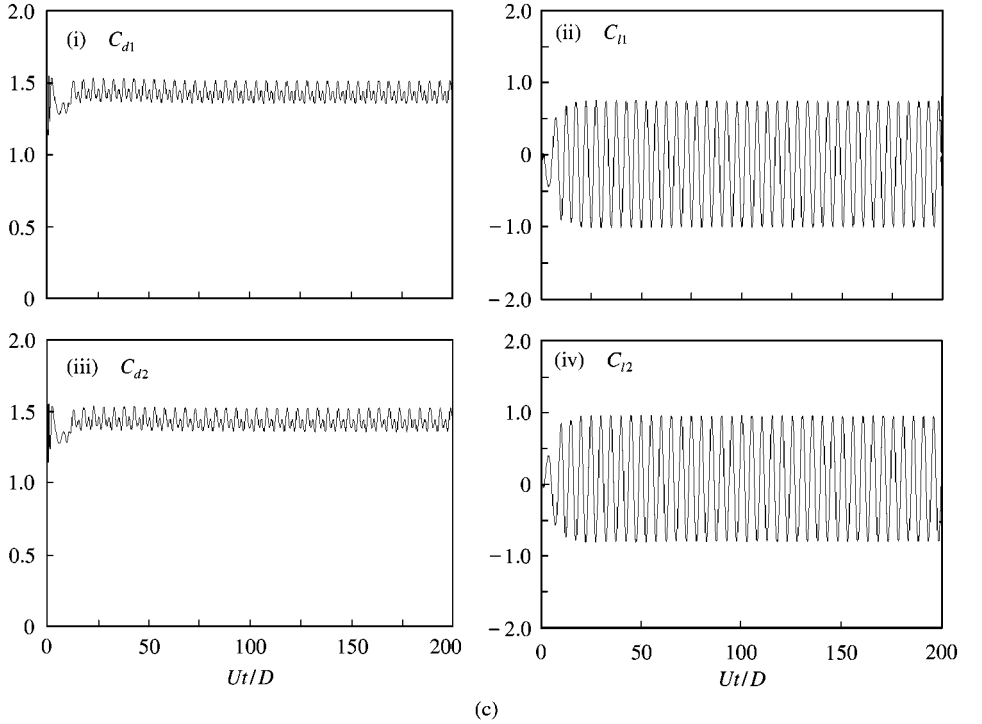

(c)

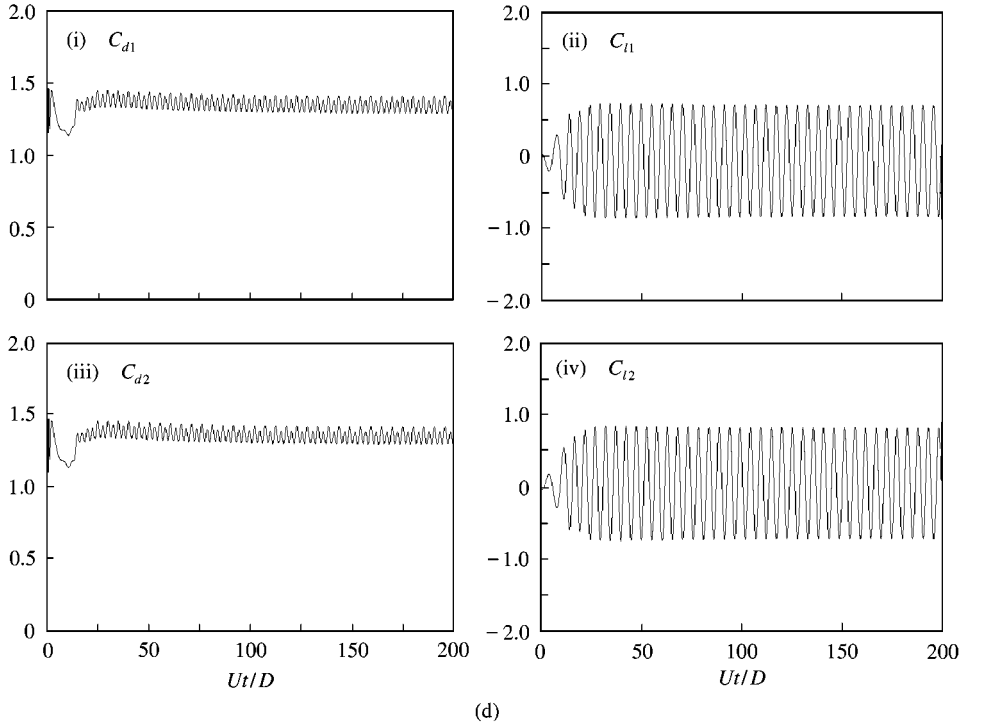

(d)

Fig. 13. (*Continued*.)

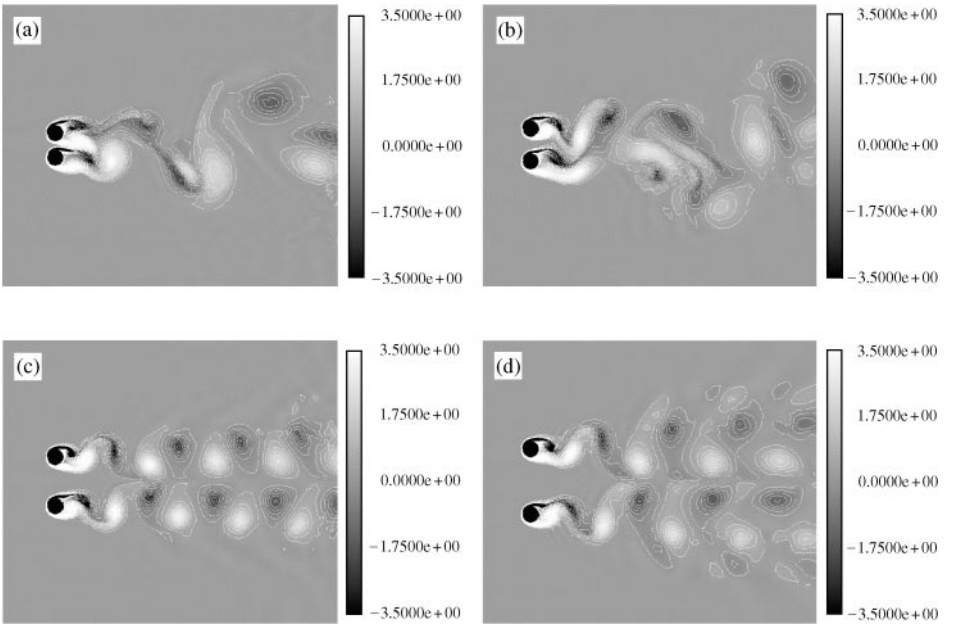

Figure 16. Vorticity contours, side-by-side arrangement (Re = 200). (a) $L = 1{\cdot}5D$, (b) $2D$, (c) $3D$, and (d) $4D$.

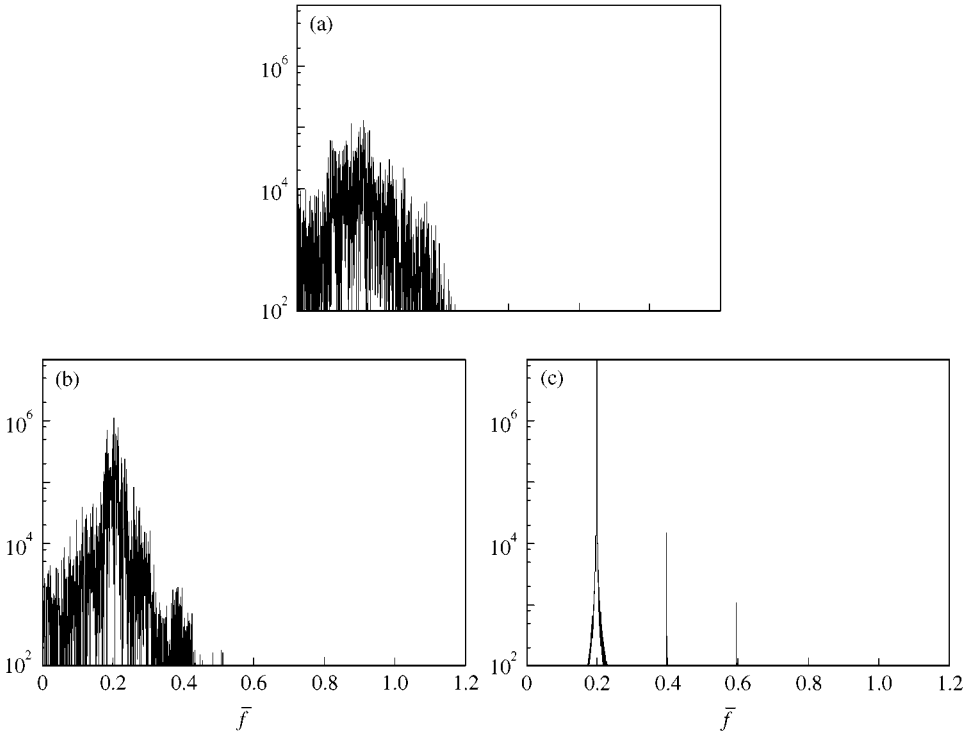

Figure 17. Power spectrum of the lift coefficient, side-by-side arrangement. (a) $L = 1.5D$, (b) $2D$, and (c) $3D$.

TABLE 6
Average drag coefficient, lift coefficients and Strouhal number for the side-by-side configuration, index 1 refers to the upper cylinder and index 2 to the lower cylinder

Gap	$C_{d_{m1}}$	$C_{d_{m2}}$	$C_{l_{m1}}$	$C_{l_{m2}}$
1·5D	1·32	1·32	−0·40	0·40
2D	1·42	1·42	−0·22	0·22
3D	1·41	1·41	−0·10	0·10
4D	1·34	1·34	−0·05	0·05

observed for the gaps in this range. However, the time scale was considerably shorter than that observed by Kim & Durbin (1988). For gaps above 3D, both cylinders shed vortices synchronized and in anti-phase. For a gap $L = 3D$, the power-spectrum estimation of the lift coefficient showed a very distinctive peak at the Strouhal frequency, and the presence of sub-harmonics. In the range where the "flopping" phenomenon has been observed, i.e., for gaps $L \leq 2D$, power spectra are broad-banded with a peak, not remarkably sharp, located at $\bar{f} \simeq 0{\cdot}2$.

ACKNOWLEDGEMENTS

The authors are grateful to FAPESP (grant 98/11530-9 and 94/3528-3) and PETROBRAS (The Brazilian State Oil Company) for providing them a Research Grant for this project and CNPq for a partial Grant. The LCCA (USP - Brazil) provided the computational facilities for some flow visualizations presented in this paper. Part of those have been prepared by the graduate student Ricardo B. Flatschart and the under-graduate students Arthur Leotta and Cassio T. Yamamoto, whom we would like to thank.

REFERENCES

ARIE, M., KIYA, M., MORIYA, M. & MORI, H. 1983 Pressure fluctuations on the surface of two cylinders in tandem arrangement, *ASME Journal of Fluids Engineering* **105,** 161–167.

ARKELL, RICHARD, H. 1997 Private communication.

ARKELL, R. H. 1995 Wake dynamics of cylinders encountering free surface gravity waves, Ph.D. thesis, University of London, U.K.

BARRETT, R. *et al.* 1992. *Templates for the solution of linear systems: building blocks for iterative methods.*

BATCHELOR, G. K. 1967 *An Introduction to Fluid Dynamics* Cambridge: Cambridge University Press.

BEARMAN, P. W. & WADCOCK, A. J. 1973 The interaction between a pair of circular cylinders normal to a stream. *Journal of Fluid Mechanics* **61,** 499–511.

BORTHWICK, A. 1986 Comparison between two finite-difference schemes for computing the flow around a cylinder. *International Journal for Numerical Methods in Fluids* **6,** 275.

BRAZA, M., CHASSAING, P. & HA MINH, H. 1986 Numerical study and physical analysis of the pressure and velocity fields in the near wake of a circular cylinder, *Journal of Fluid Mechanics* **165,** 79–130.

BREZZI, F. & FORTIN, M. 1991 *Mixed and Hybrid Finite Element Methods* New York: Springer-Verlag.

BROOKS, A. N. & HUGHES, T. J. R. 1982 Streamline Upwind/Petrov–Galerkin formulations for convection dominated flows with particular emphasis on the incompressible Navier–Stokes equations. *Computer Methods in Applied Mechanics and Engineering* **32,** 199–259.

DOLAN, P. S., GRAHAM, J. M. R. & YOUNG, J. A. 1990 Computational of unsteady two-dimensional separated flow using a hybrid mesh technique. *Proceedings International Symposium on Non-steady Fluid Dynamics* (eds J. A Miller & D. P. Telionis), Book No. H00597-1990. New York: ASME.

GIANNAKIDIS, G. 1997 Private communication.

Gresho, P. M., Chan, S. T., Lee, R. L. & Upson, C. D. 1984 A modified finite element method for solving the time-dependent, incompressible Navier–Stokes equations. Part 1: Theory. *International Journal for Numerical Methods in Fluids* **4,** 557–598.

Karniadakis, G. E. & Triantafyllou, G. 1989 Frequency selection and asymptotic states in laminar wake. *Journal of Fluid Mechanics* **199,** 441–469.

Kim, H. J. & Durbin, P. A. 1988 Investigation of the flow between a pair of cylinders in the flopping regime, *Journal of Fluid Mechanics*, **196,** 431–448.

Koschel, W., Lotzerich, M. & Vornberger, A. 1989 Solution on unstructured grids for the Euler and Navier Stokes equations. AGARD, CP-437, Vol. 1, pp. 1–26.

Lecointe, Y. & Piquet, J. 1988 *Numerical methods for unsteady flows.* VKI Lectures.

Martinez, G. 1979 Character of the flow around a circular cylinder at moderate Re. Ph.D. thesis, Institut. National Poytechnique, Toulouse, France.

Manna, M. 1997 *Introduction to the Modelling of Turbulence.* von Karman Institute for Fluid Dynamics, Lecture Series 1997-03, Belgium.

Meling, T. S. & Dalheim, J. 1997 Numerical Prediction of the Response of a Vortex-Excited Cylinder at Low Reynolds Numbers. *Proceedings* 7th *International Offshore and Polar Engineering Conference* (*ISOPE* 97), Honolulu, U.S.A.

Meneghini, J. R. 1993 Numerical simulation of bluff body flow control using a discrete vortex method. Ph.D. thesis, University of London, U.K.

Mittal, S., Kumar, V. & Raghuvanshi, A. 1997 Unsteady incompressible flows past two cylinders in tandem and staggered arrangements. *International Journal for Numerical Methods in Fluids* **25,** 1315–1344.

Ng, C. W. & Ko, N. W. M. 1995 Flow interaction behind two circular cylinders of equal diameter — a numerical study. *Journal of Wind Engineering and Industrial Aerodynamics* **54/55,** 277–287.

Norberg, C. 1993 Private communication.

Roshko, A. 1954 On the drag and shedding frequency of two dimensional bluff bodies. Technical Note 3169, *National Advisory Committee for Aeronautics* (*NACA*), Washington.

Sa, J. Y. & Chang, K. S. 1991 Shedding patterns of the near-wake vortices behind a circular cylinder. *International Journal for Numerical Methods in Fluids* **12,** 463–474.

Saltara, F. 1999 Numerical Simulation of the flow about circular cylinders, Ph.D. thesis, EPUSP University of São Paulo, Brazil (in Portuguese).

Shariff, K., Pulliam, T. H. & Ottino, J. M. 1990 A dynamical systems analysis of kinematics in the time-periodic wake of a circular cylinder. In *Vortex Dynamics and Vortex Methods*, (eds C. R. Anderson and C. Greengard), Lectures in Applied Mathematics, Vol. 28, American Mathematical Society, 613–646.

Slaouti, A. & Stansby, P. K. 1992 *Journal of Fluids and Structures* **6,** pp. 641–670.

Stansby, P. K. & Slaouti, A. 1993 Simulation of vortex shedding including blockage by the random vortex and other methods. *International Journal for Numerical Methods in Fluids* **17,** 1003–1013.

Siqueira, C. L. R., Meneghini, J. R. & Saltara, F. 2000 Three-dimensional simulation of the flow past a circular cylinder at low Reynolds numbers. Submitted for presentation in the IUTAM Symposium on Bluff Body Wakes and Vortex-Induced Vibrations (BBVIV2), 13–16 June 2000, Marseille, France.

Summer, D., Price, S. J. & Païdoussis, M. P. 1998 Investigation of side-by-side circular cylinders in steady cross-flow by particle image velocimetry. *Proceedings 1988 ASME Fluids Eng. Division Summer Meeting* (eds P. W. Bearman & H. K. Williamson), Paper 37.

Tritton, D. J., 1959 *Journal of Fluid Mechanics* **6,** 547–567.

Williamson, C. H. K. 1985 Evolution of a single wake behind a pair of bluff bodies. *Journal of Fluid Mechanics* **159,** 1–18.

Williamson, C. H. K. 1991 2-D and 3-D aspects of the wake of a cylinder, and their relation to wake computations. In *Vortex Dynamics and Vortex Methods* (eds C. R. Anderson and C. Greengard, Lectures in Applied Mathematics, Vol. 28, American Mathematical Society, pp. 719–751.

Young, D.-L. & Ni, W.-B. 1989 Penalty finite element applications to flow problems. *Department of Civil Engineering Report*, National Taiwan University, Taipei, R.O.C.

Zdravkovich, M. M. 1987 The effects of interference between circular cylinders in cross flow. *Journal of Fluids and Structures* **1,** pp. 239–261.

Zdravkovich, M. M. 1977 Review of flow interference between two circular cylinders in various arrangements, *ASME Journal of Fluids Engineering* **99,** 618–633.

Zienkiewicz, O. C. & Morgan, K. 1983 *Finite Elements and Approximation.* New York: John Wiley and Sons.

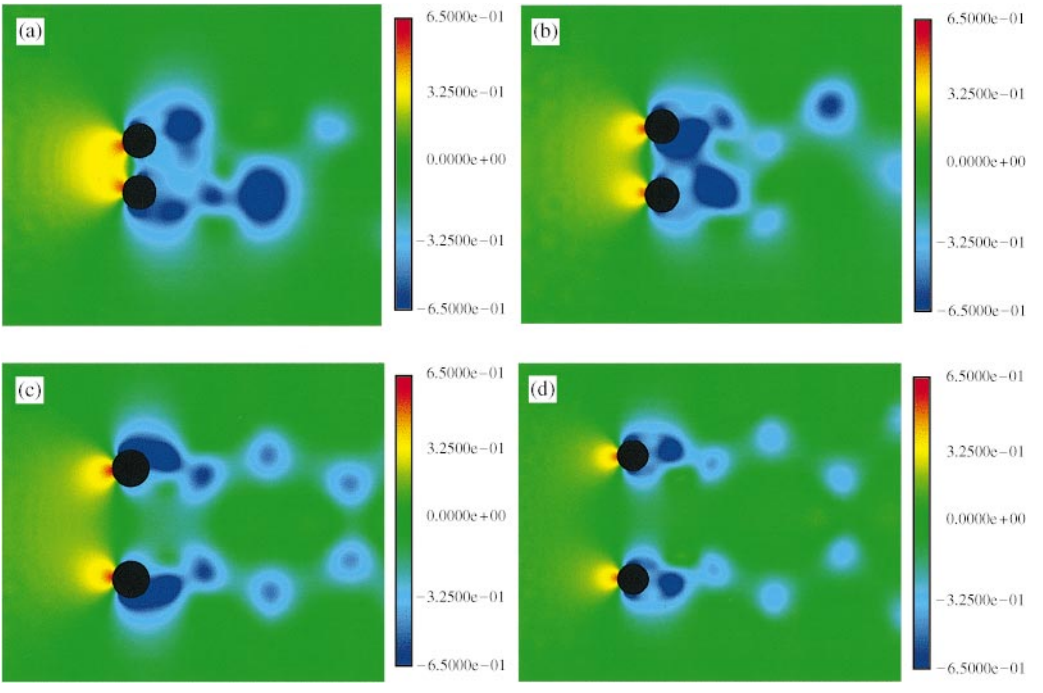

Figure 14. Pressure contours, side-by-side arrangement (Re = 200). (a) $L = 1{\cdot}5D$, (b) $2D$, (c) $3D$, and (d) $4D$.

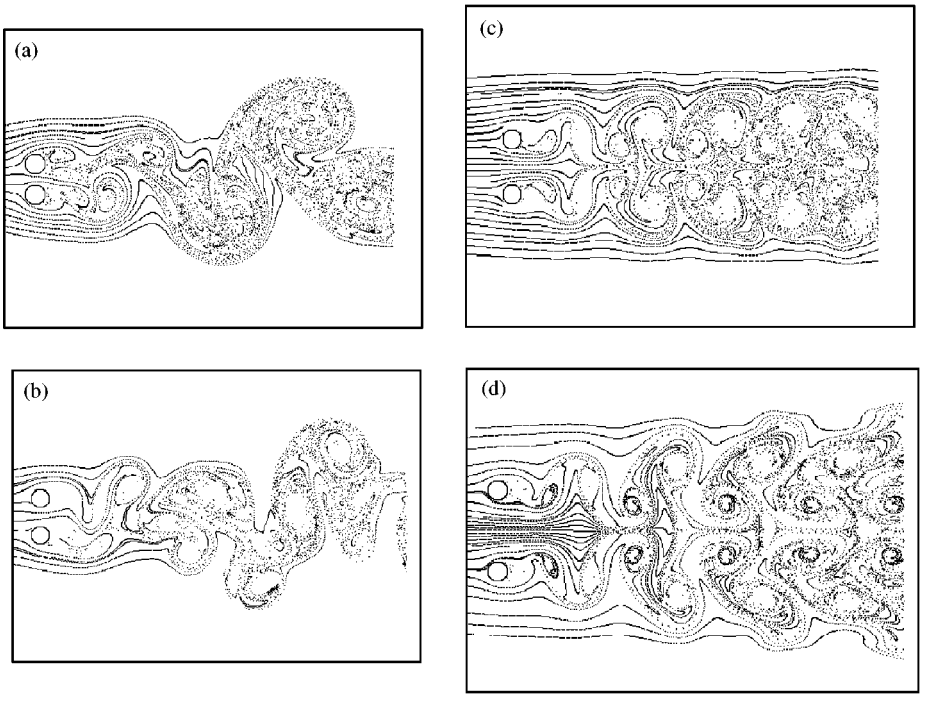

Figure 15. Wake represented by streaklines, side-by-side arrangement (Re = 200). (a) $L = 1.5D$, (b) $2D$, (c) $3D$, and (d) $4D$.